STUDY OF ATMOSPHERIC STABILITY INDICES FORECAST FOR IDENTIFYING CONVECTIVE ACTIVITY IN THE BANDUNG BASIN BASED ON THE WRF-ARW MODEL AND THRESHOLD EXCEEDANCE

Abdul Hamid Al Habib[1,3]*, Reinhart C. H. Hutauruk[1,3], Nurjanna Joko Trilaksono[2], Haryas Subyantara Wicaksana[3], Arini Amalia Choir[4]

[1] Graduate Programme in Earth Science, Faculty of Earth Sciences and Technology, Bandung Institute of Technology (ITB), Bandung, Indonesia.

[2] Atmospheric Science Research Group, Faculty of Earth Sciences and Technology, Bandung Institute of Technology (ITB), Bandung, Indonesia

[3] Meteorology, Climatology, and Geophysical Agency (BMKG), Jakarta, Indonesia

[4] Faculty of Mathematics and Natural Sciences, Bandung Institute of Technology (ITB), Bandung, Indonesia

*****E-mail: jpatiani@itb.ac.id*

Received: November 3, 2024 Reviewed: March 13, 2025 Accepted: December 15, 2025

ABSTRACT

The Bandung Basin, characterized by complex topography, experiences some of the highest occurrences of heavy rainfall and hail in Indonesia. This study focuses on forecasting convective activity associated with the thunderstorm and heavy rainfall event that triggered flooding in the Pagarsih area, West Java, on 4 October 2022. The spatiotemporal forecast characteristics of convection are assessed using atmospheric stability indices (CAPE, K Index, Total Totals Index, and Lifted Index), together with low-level convergence and updraft fields from the WRF-ARW model, to identify the development of convective cells influenced by the Bandung Basin's topography. The results reveal a distinct spatiotemporal evolution of convection across mountainous and valley regions. In the early phase, convection first emerged over the mountainous area, driven by a gradual increase in atmospheric instability and low-level convergence, before developing over the valley. The forecasted stability indices display a rising trend 2–5 hours before the onset of thunderstorms and heavy rainfall in the Pagarsih area. At the mature stage, mountain convection was mainly initiated by solar radiation heating, while valley convection was predominantly triggered by mechanical forcing, characterized by a sudden surge in low-level convergence, instability indices, and updraft, leading to more explosive convective development. During dissipation, convection weakened in both regions, but the mountainous area showed stronger convective recovery, indicating higher sensitivity to surface reheating.

Keywords: Convective Activity, Atmospheric Stability Indices, WRF-ARW

1. Introduction

From 2010 to 2023, the Bandung Basin in West Java recorded the highest frequency of extreme weather events (heavy rainfall and hail) compared to other regions in Indonesia [1]. The Bandung Basin is a bowl-shaped area located in West Java Province, surrounded by mountain ranges to the north, south, and east, forming a complex topography. This region is particularly significant because it is frequently affected by hydrometeorological disasters, including floods that can be triggered by heavy rainfall, causing infrastructure damage and socio-economic losses, especially in densely populated urban areas such as Bandung and Cimahi.

The Pagarsih area in Bandung City has been recorded as one of the most frequently and severely flooded regions due to heavy rainfall. According to online media reports, this area has experienced flash flooding with water levels reaching approximately 1 meter, the highest among other locations in the city [2]. Furthermore, Pagarsih was listed among 16 flood-prone points during the 2018 rainy season, with at least five flooding events reported [3]. One significant instance of heavy rainfall that triggered flooding in this area occurred on October 4, 2022 [4].

Identifying the factors that cause extreme weather (heavy rainfall) can guide forecasters in predicting these events [5]. Previous studies have shown that convective activity increases sharply several hours before extreme weather occurs [6,7,8]. This convective activity is triggered by atmospheric instability [9,10,11], which can be quantified using atmospheric stability indices. However, most previous studies on atmospheric stability indices have been conducted in subtropical or mid-latitude regions [9,10,11], where convective dynamics and thermodynamic structures differ significantly from those in tropical areas like

Indonesia. Tropical regions are generally characterized by warmer near-surface temperatures and higher moisture content, leading to stronger buoyancy and more frequent deep convection, even under conditions of moderate atmospheric instability [11,12].

Atmospheric stability indices are widely recognized as key predictors of thunderstorm development [10–13]. However, their operational use is often constrained by the limited spatial and temporal coverage of radiosonde observations. To address this, the present study evaluates model-derived stability indices as a forecasting tool for convective activity.

Advances in numerical weather prediction have improved the ability to simulate convective clouds and mesoscale processes, which are essential for regions like Indonesia where weather patterns are shaped by multiscale sea–land and local–global interactions [14]. Among available models, WRF has demonstrated better performance than GFS [15] and is therefore suitable for diagnosing extreme convective events such as thunderstorms and heavy rainfall [16].

Earlier studies, based on WRF analyses, soundings, or satellite data have shown that convection over the Bandung Basin often initiates over the northern and southern mountains via low-level convergence, and later regenerates over the valley through cold-pool interactions with warm air [17–19]. While model-based stability index forecasts have proven effective as early indicators of thunderstorms in the tropics [7], [20], [21], their predictive application in complex terrain remains limited. Therefore, this study employs WRF forecast data to identify the spatiotemporal evolution of convection through atmospheric stability indices, providing a predictive framework to anticipate convective development under the Basin's distinct topographic influence.

2. Methods

This study analyzes convective activity during thunderstorms on October 4, 2022, which were accompanied by heavy rainfall and triggered flooding in the Pagarsih area (Bandung). The WRF-ARW model setup uses the WRF Domain Wizard during the WPS process to simplify domain definition, namelist generation, and automatic WPS execution.

The WRF-ARW model version 4.5.3 was selected to utilize recent physics and stability enhancements over version 4.4.2. The model was run using one parent domain and a three-domain configuration (with two levels of nesting), as shown in Figure 1. The parameterization scheme used in this study follows the approach developed by Smith et al. [22]. Table 1 summarizes the model configuration parameters applied in this research. Smith et al. [22] examined the impact of topographic modification on convective regeneration and found that modified topography failed to produce convective regeneration, whereas unmodified topography did. Based on these findings, the parameterization scheme from Smith et al. [22] was adopted in the WRF model to investigate convective activity in the Bandung Basin, with atmospheric stability indices used to identify and understand convective processes over complex terrain.

The input data for the WRF-ARW model consists of Global Forecasting System (GFS) data from October 3, 2022, at 12 UTC to October 4, 2022, at 12 UTC. This GFS data, available at https://nomads.ncdc.noaa.gov/data/gfs4/, has a spatial resolution of 0.25° x 0.25° and a temporal resolution of 3 hours. The data used for the simulation spans 24 hours, including 12 hours for spin-up and 12 hours for analyzing the event.

Table 1. Configuration of the WRF-ARW model

Arrangement Running WRF	**Information**		
	Domain 1 (9 km)	**Domain 2 (3 km)**	**Domain 3 (1 km)**
Temporal Resolution	1 hour		
e_we	128	142	229
e_sn	87	112	250
ra_sw_physics	Dudhia		
ra_lw_physics	Rapid Radiative Transfer Model		
bl_pbl_physics	Yonsei University scheme		
cu_physics	BMJ	-	-
mp_physics	Morrison (double Moment)		
land_surface	5–layer Thermal Diffusion		
surface_layer	Standard Monin-Obukhov similarity functions		

Rainfall observation data from the Husein Sastranegara Weather Observation Station in Bandung, which is the closest station to the Pagarsih area, were used to analyze the timing of thunderstorms and heavy rainfall events (Figure 1). On October 4, 2022, cumulonimbus clouds with thunderstorms were observed at 05:30 UTC, followed by heavy rainfall until 06:00 UTC [23]. In addition, due to the unavailability of radar data at the event location, validation was conducted using Himawari satellite data obtained from the Center for Environmental Remote Sensing (CEReS), Chiba University, Japan [24]. The Himawari satellite data used in this study were brightness temperature (BT) values representing cloud-top temperatures from Band 13 (10.4 μm), with a spatial resolution of 2 km.

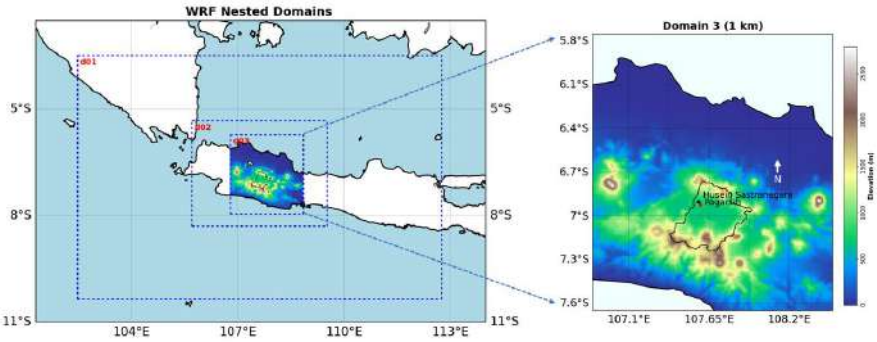

Figure 1. WRF-ARW domain setup. Black dot: Husein Sastranegara Airport; red dot: Pagarsih, Bandung.

This study focuses on four primary stability indices: Convective Available Potential Energy (CAPE), Lifted Index (LI), K-Index (KI), and Total Totals Index (TT), selected for their effectiveness in capturing different aspects of atmospheric instability. These indices are widely used in tropical region and ease of computation from standard upper-air data [6], [7], [20], [21].

a) CAPE (*Convective Available Potential Energy*)

CAPE represents the amount of buoyant energy available to accelerate an air parcel upward through the atmosphere. It is calculated as the vertical integral of positive buoyancy, defined by the virtual temperature difference between the parcel (T_{vp}) and its environment (T_{ve}), from the level of free convection (LFC) to the level of neutral buoyancy (LNB) [22, 25]. The mathematical expression for CAPE is given as:

$$CAPE = \int_{LFC}^{LNB} R_d\left(T_{vp} - T_{ve}\right) d\ln(p) \qquad (1)$$

b) LI (Lifted Index)

Lifted Index (LI) was discovered by Joe Galway [26] by lifting air in the boundary layer near the surface until it reaches the 500 mb layer, then comparing the temperature of the lifted air parcel ($Tvp(\text{surface})$) with the temperature of the environment ($Tve(500\ \text{hPa})$). LI can be calculated using the following equation:

$$\text{Lifted Index} = Tvp(\text{surface}) - Tve(500\ \text{hPa}) \qquad (2)$$

c) KI (K-Index)

The K-index can be used to see air instability, opportunities for convective cloud growth and thunderstorms. The K-index is usually calculated based on temperature, dew point at several air pressure levels in the atmosphere. The following is the KI formula [10]:

$$KI = (T_{850} - T_{500}) + Td_{850} - (T_{700} - Td_{700}) \qquad (3)$$

Information:

T850 : temperature at 850 hPa
T700 : temperature at 700 hPa
T500 : temperature at 700 hPa
Td850: dew point at 850 hPa
Td700: dew point at 700 hPa

d) TT (Total-totals Index)

The Total Totals Index (TT) is a meteorological measure for assessing atmospheric stability developed by the U.S. Air Force [27], TT combines the Cross Totals Index and Vertical Totals Index using temperature (T) and dew point temperature (Td) data from the 850 mb and 500 mb layers. TT-Index can be calculated using the following equation:

$$TT = Td_{850} - T_{500} + T_{850} - T_{500} \qquad (4)$$

Information:

Td850 : dew point at 850 hPa
T850 : temperature at the 850 hPa
T500 : temperature at the 500 hPa

2. Result and Discussion

Figure 2 shows that WRF-derived CTT closely matches Himawari-9 IR data from 03–06 UTC, confirming the modeled convective evolution over the Bandung Basin. Convection initiated over the northern and southern mountains at 03 UTC, expanded into the northwestern valley by 04 UTC, and peaked at 05 UTC, with CTT cooling to −75 to −80 °C in the model and −21 to −24 °C in the satellite. By 06 UTC, the coldest cloud tops were centered over the Pagarsih valley, indicating sustained deep convection. The model slightly overestimated cell numbers and displaced them eastward, but still captured the main spatiotemporal progression (from initiation to dissipation across mountains and valley) supporting further identification of the full convective life cycle.

Based on Figures 2–4, between 03 and 04 UTC, the convective system CS(m) over the northern and southern mountains of the Bandung Basin was driven by a combination of solar heating, upslope wind convergence, and increasing instability indices. At 03 UTC, mechanical lifting over the terrain led to adiabatic ascent and enhanced buoyancy, while mid-level moistening elevated the K Index and Total Totals (Figure 3c.1 and 3d.1). Meanwhile, the valley region remained relatively stable due to insufficient moisture and dynamic lifting.

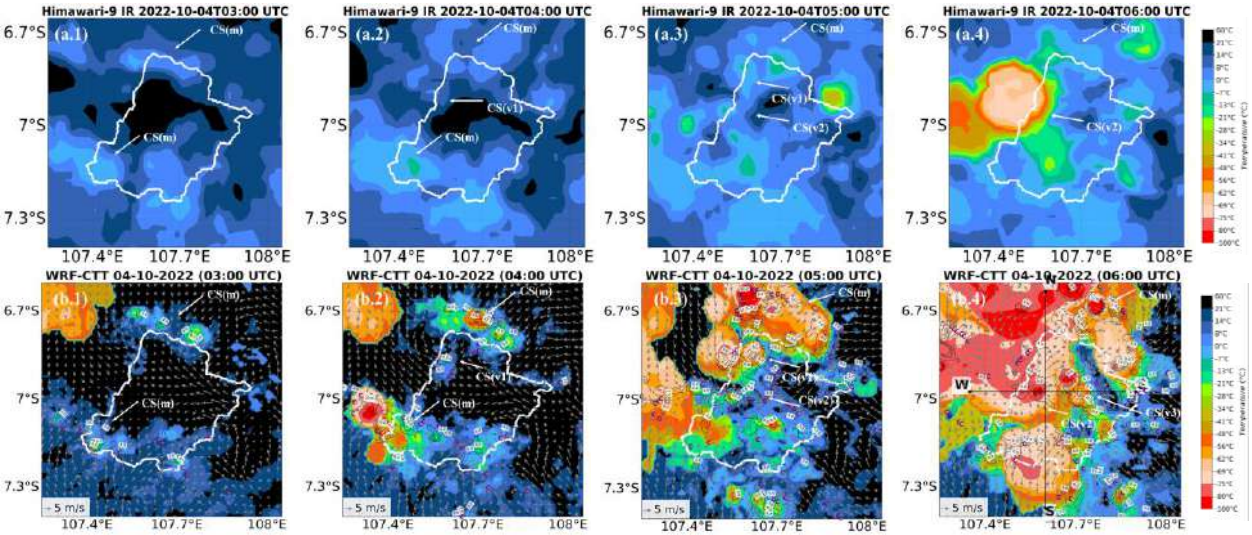

Figure 2. (a) Himawari-9 IR cloud-top temperatures (°C, shaded); (b) WRF-ARW cloud-top temperatures (°C, shaded) and vertical velocity (m/s, black contours with label), wind vector at the lowest level of the model (~ 25 m) and convergence zones (divergence ≤ –0.0035 s^{-1}, blue C symbols). White contours indicate the Bandung Basin boundaries. CS(m) represents convective systems in the mountainous region, while CS(v) represents convective systems in the valley. The vertical and horizontal black lines indicate the area selected for the cross-section sample, with their intersection point representing the Pagarsih region.

By 04 UTC, instability intensified and expanded toward the valley, with a low-level convergence (LLC) zone forming over Pagarsih as near-surface winds (~25 m) from the north, northwest, and southeast intersected through mountain gaps. This wind layer effectively captures terrain-modified boundary-layer flows and convergence features that are crucial for convective initiation. Although buoyancy remained weak, as indicated by low CAPE and LI, the increasing KI and TT values reflected growing mid-level moist instability (Figure 3), marking the early stage of convective development over the Pagarsih valley (CS(v1)) (Figure 4c.2 and 4d.2). These results align with previous findings highlighting the role of terrain-induced lifting in convection [29] and the importance of LLC in triggering deep convection over complex topography [30]

At 05 UTC, a stronger convergence zone formed over the Pagarsih region as northerly and southerly winds merged through mountain gaps from the west, northeast, and east, triggering a new updraft. At the earlier CS(v1) site (at 04 UTC), CAPE, LI, KI, and TT decreased due to evaporative cooling, stabilizing the atmosphere (Figure 4 c.3, d.3). As CS(v1) decayed, its outflow boundaries generated a new convergence zone along the southern flank over lower terrain (Figures 3–4). Simultaneously, downslope winds from both mountain ranges descended into the basin, reinforcing low-level convergence. At this new zone, CAPE sharply increased, LI became more negative, and KI–TT rose, indicating saturated parcels rapidly lifted by convergence and diurnal heating. This enhanced mid-level instability supported the development of a stronger convective cell, CS(v2), over the Pagarsih region, producing thunderstorms and heavy rainfall with intensified vertical motion (Figure 2 b.3). This process aligns with studies showing that cold-pool outflows from weakening storms commonly trigger secondary convection via localized convergence and frontogenesis [31].

Based on Figure 3, at 06 UTC a marked decrease in all atmospheric stability indices (CAPE, LI, KI, and TT) was observed over areas that had previously experienced intense convective activity, particularly the west-central valley CS(v2) and the northern mountainous region CS(m). This decline reflects a post-convective stabilization process, in which latent heat release during deep convection, followed by precipitation-induced evaporative cooling, reduces instability in both the lower and mid-troposphere. As the CS(m) and CS(v2) cells began to dissipate, the surrounding environment became increasingly stable due to cooling and a more homogenized vertical temperature profile, suppressing parcel lifting and inhibiting further convective initiation.

However, pockets of moderate instability persisted along the western and eastern flanks of the former CS(v2) region (Figure 3a.4, d.4; Figure 4a.4, c.4), indicating that convective potential had not completely vanished. These areas remained conditionally unstable, likely influenced by a surface-based cold pool generated by previous heavy precipitation (Figure 4d.4). As the cold pool advances, interactions between its leading edge (CPLE) and the surrounding warmer air can trigger convective regeneration, such as CS(v3), through lifting along the density current boundary [19], consistent with findings by Firdaus et al. [19] showing that intense rainfall over the central basin produces cold pools spreading both eastward and westward.

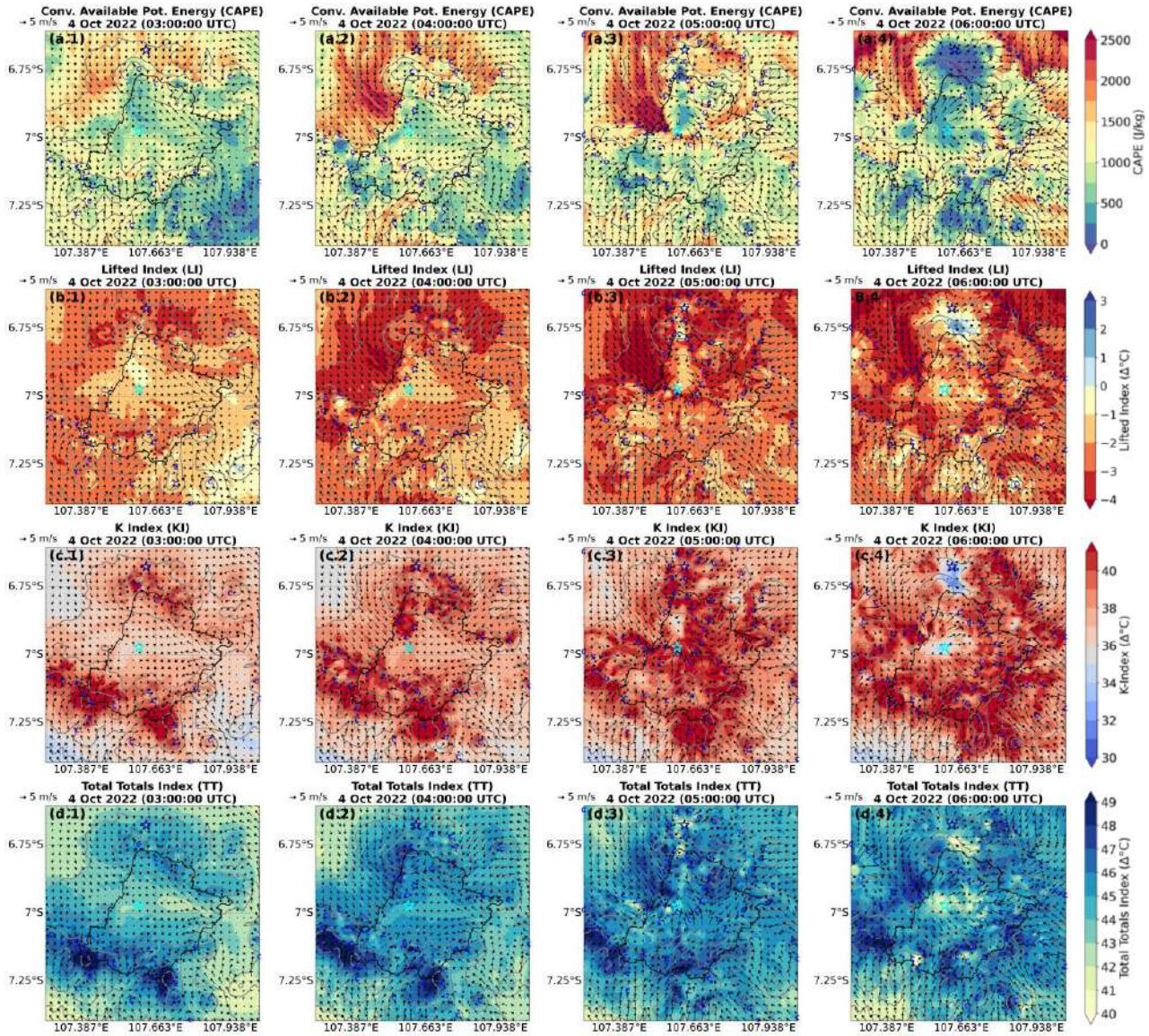

Figure 3. Spatial distribution of stability indices over the Bandung Basin: (a) CAPE, (b) LI, (c) KI, (d) TT (Δ°C, shaded), with the wind vector at the lowest level of the model (~ 25 m) and convergence zones (divergence ≤ – 0.0035 s^{-1}, blue C symbols). Black contours indicate the Bandung Basin boundaries. Dark blue and cyan stars mark representative points of convective cells in north mountain region and valley (Pagarsih region), respectively.

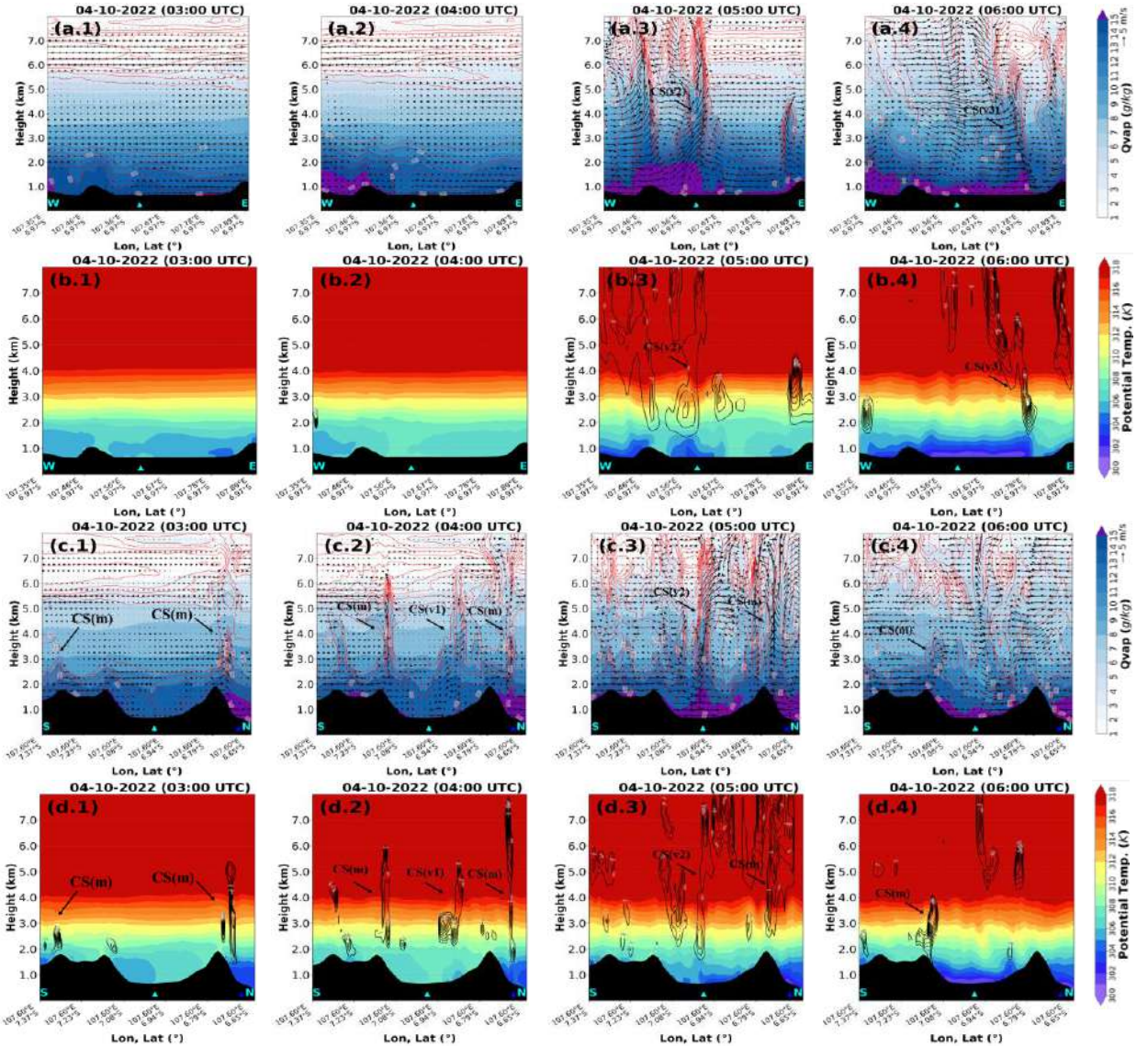

Figure 4. Vertical cross-sections of the convective cell from Figure 2: (a, c) Water vapor mixing ratio (shaded), equivalent potential temperature (red contours), and wind vectors for zonal (a) and meridional (c) components. (b, d) Potential temperature (shaded) and cloud mixing ratio contours for zonal (b) and meridional (d) components. CS(m) represents convective systems in the mountainous region, while CS(v) represents convective systems in the valley. Dark blue and cyan triangles representative points of convective cells in north mountain region and Pagarsih valley region, respectively.

Based on the time series of atmospheric stability indices, minimum divergence, and maximum updraft (Figure 5), the pre-convective stage between 00 and 04 UTC was characterized by a gradual build-up of thermodynamic instability that preceded the strengthening of LLC and vertical motion. Gradual solar heating over the northern Bandung mountains enhanced boundary-layer warming and moisture accumulation, leading to a steady rise in instability, as indicated by increasing CAPE (from 547 to 1746 J/kg) and increasingly negative Lifted Index values (from –1.25 °C to –3.29 °C). During this phase, updrafts remained weak (<1 m/s) and LLC was still modest, showing that instability developed earlier than the dynamical response.

The convective system reached its mature stage between 05 and 06 UTC, when the previously accumulated instability began to be released. Although CAPE had already started to decrease (from 1746 to 1170 J/kg), dynamic forcing intensified: updraft speed surged to 9.1 m/s at 05 UTC, coinciding with the strongest LLC (minimum divergence -3.26×10^{-3} s^{-1}). This temporal sequence confirms that the thermodynamic preconditioning acted as the main trigger, while mechanical forcing accelerated the explosive growth of the convective core. At 06 UTC, both thermodynamic and dynamic supports weakened simultaneously, divergence values became less negative, and updraft strength fell to 1.2 m/s, indicating the onset of the dissipation phase as surface heating weakened and convective cells decayed. After dissipation, convection recovered faster over the mountains than in the valley due to renewed surface heating (Figure 5).

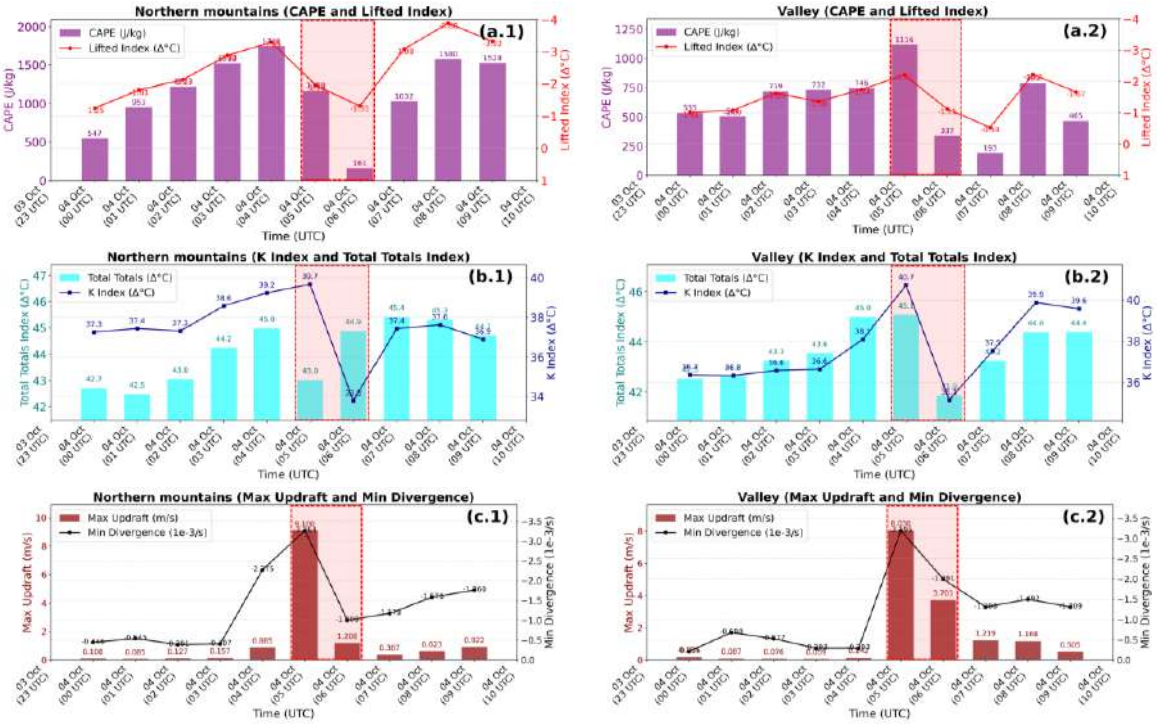

Figure 5. Time series of stability indices derived from the average of the nearest grid points around the dark blue and cyan stars shown in Figure 3, which mark locations over the mountains (left) and the valley (right). Red shading indicates the mature-to-dissipation phase of the convective cell..

The temporal evolution of atmospheric stability indices over the Pagarsih (valley region) shows a clear pre-storm signal, with instability intensifying 2–5 hours before the thunderstorm and heavy rainfall at 05:30–06:00 UTC (Figure 5). From 00 to 04 UTC, CAPE steadily increases from ~530 to ~746 J/kg, accompanied by rising KI and TT and slightly negative LI, indicating growing convective potential. At 05 UTC, instability surges sharply (CAPE 1116 J/kg, KI 40.7 Δ°C, TT 45.1 Δ°C), coinciding with strong LLC (divergence -3.19×10^{-3} s^{-1}) and a rapid increase in updraft (8.03 m/s), marking the onset of deep convection that later produced thunderstorm and heavy rainfall. At 06 UTC, all indices weaken (CAPE 337 J/kg, KI 35 Δ°C), along with reduced LLC (-1.99×10^{-3} s^{-1}) and updraft (3.7 m/s), indicating post-storm stabilization. These results indicate that the most pronounced interaction between LLC and vertical motion took place about one hour prior to the storm, underscoring the importance of mechanically driven convergence in enhancing pre-storm atmospheric instability in the valley environment.

3. Conclusion

This study shows that convective development in the Bandung Basin is strongly shaped by its complex topography. The WRF-ARW model captured a 2–5 hours pre-storm increase in atmospheric instability over the Pagarsih valley before thunderstorms and heavy rainfall occurred. Mountain convection was mainly driven by daytime solar heating, whereas valley convection was dominated by mechanically induced low-level convergence. During dissipation, convection weakened in both regions, but recovered earlier over the mountains due to stronger sensitivity to renewed surface heating.

Suggestion

Future studies should define threshold values of WRF-based stability indices for thunderstorm prediction, validate them with radiosonde data for Meteorology, Climatology, and Geophysics Agency (BMKG) operations, expand case studies, and assess the use of WRF-derived indices as predictors in AI models for forecasting extreme convective events.

Acknowledgments

This research was funded by Indonesia Endowment Fund for Education Agency (LPDP). We thank to BMKG for providing rain gauge data free of charge. In addition, thanks also go to the Bandung Institute of Technology (ITB) for providing the server facilities for running the WRF-ARW model in this research.

References

[1] Badan Meteorologi, Klimatologi, dan Geofisika. *Portal Informasi Kejadian Cuaca Ekstrem (PIKACU)*. Retrieved July 26, 2025, from https://pikacu.bmkg.go.id/.

[2] Detikcom. "*Ini 23 wilayah di Bandung yang langganan banjir 'cileuncang'*," Retrieved July 26, 2025, from https://news.detik.com/berita-jawa-barat/d-3070467/ini-23-wilayah-di-bandung-yang-langganan-banjir-i-cileuncang-i

[3] Kompas. "*16 Titik di Kota Bandung Rawan Banjir*," Retrieved July 26, 2025, from https://regional.kompas.com/read/2018/03/09/13531391/16-titik-di-kota-bandung-rawan-banjir.

[4] SuaraJabar. "*Hujan deras guyur sore ini, banjir*

terjang Jalan Pagarsih dan Cimahi, arus lalu lintas macet." Retrieved July 26, 2025, from https://jabar.suara.com.
[5] A. Zakir, *Modul Diklat Meteorologi Publik*, Jakarta: Pusat Pendidikan dan Pelatihan BMKG, 2010.
[6] A. H. Al Habib, E. Bangalino, M. Ryan, "Rancang Bangun Model Artificial Neural Network Untuk Prediksi Probabilistik Kejadian Thunderstorm di Wilayah Manado," *Prosiding Seminar Nasional Sains Atmosfer*, 2020.
[7] J. Ferdaus, et al., "Prediction of Thunderstorms based on Atmospheric Instability Indices over Bangladesh using WRF-ARW Model," *JALAWAAYU*, Vol. 1(2), 2021.
[8] Williams, E. R., et al., "The behavior of total lightning activity in severe Florida thunderstorms," *Atmospheric Research*, 51(3), 245–265. 1999.
[9] D. DeRubertis, "Recent Trends in Four Common Stability Indices Derived from U.S. Radiosonde Observations," *J. Climate*, vol. 19, pp. 309–323, 2006.
[10] J.J. George, *Weather forecasting for aeronautics*, New York: Academic Press, 1960.
[11] A.J. Haklander, & A. van Delden, Thunderstorm predictors and their forecast skill for the Netherlands, *Atmospheric Research*, vol. 67– 68, pp. 273– 299, 2003.
[12] Zipser, E. J., Some views on "hot towers" after 50 years of tropical field programs and two years of TRMM data. *Cloud Systems, Hurricanes, and the Tropical Rainfall Measuring Mission (TRMM)*, 49–58.2003.
[13] P. Alford, *Tropical area prediction system (TLAPS) Guide*, Melbourne: BMTC, 1992.
[14] J. H. Qian, "Why precipitation is mostly concentrated over islands in the Maritime," *American Meteorological Society Journals*, vol. 65, pp. 1428-1441, 2008.
[15] J. T. Lestari and A. Wandala, "A study comparison of two system model performance in estimated lifted index over Indonesia," *J. Phys.*: Conf. Ser. 1025 012113, 2018.
[16] I. Gustari, et al., "Akurasi Prediksi Curah Hujan Harian Operasional Di Jabodetabek: Perbandingan Model Wrf," *Jurnal Meteorologi Dan Geofisika*, vol. 13 No. 2 Tahun 2012. Jakarta:BMKG, 2012.
[17] M. Oigawa, T. Matsuda, T. Tsuda, and Noersomadi, "Coordinated Observation and Numerical Study on a Diurnal Cycle of Tropical Convection over a Complex Topography in West Java, Indonesia," *Journal of the Meteorological Society of Japan*, vol. 95, pp. 261−281, 2017.
[18] R. Fitriani, N. J. Trilaksono, and T. W. Hadi, "Investigation of the Regeneration of Precipitating Convective Cloud in Basin Topography Area," *IOP Conf. Series: Earth and Environmental Science*, 303(012015), 2019.
[19] I. M. Firdaus, N. J. Trilaksono, and T. Yamazaki, "Mechanism of initiation and regeneration of convective cell in Bandung Basin, Indonesia," *Geosci.Lett.* 11, 44, 2024.
[20] W.-Y. Cheng, D. Kim, and R. H. Holzworth, "CAPE threshold for lightning over the tropical ocean," *Journal of Geophysical Research: Atmospheres*, vol. 126, 2021.
[21] N. Saleh, M. Gharaylou, M. M. Farahani, and O. Alizadeh, "Performance of lightning potential index, lightning threat index, and the product of CAPE and precipitation in the WRF model," *Earth and Space Science*, vol. 10, 2023.
[22] Smith, V. H., M., et al., "The role of orography in the regeneration of convection: A case study from the convective and orographically-induced precipitation study." *Meteorologische Zeitschrift*, 24(1), pp. 83-97, 2015.
[23] Meteorological, Climatological, and Geophysical Agency (BMKG) – Aviation Meteorology Center. (n.d.). *METAR/SPECI & Trend Forecast*. Retrieved July 26, 2025, from https://web-aviation.bmkg.go.id/web/metar_speci.php.
[24] Takenaka et al. "*Geolocation correction for geostationary satellite observations by phase-only correlation method using visible channel*," Remote Sensing, 12(15), 2472. 2020.
[25] K.A. Emanuel, J. D. Neelin, and C.S. Bretherton, "On large-scale circulations in convecting atmospheres," *Quarterly Journal of the Royal Meteorological Society*, vol. 120(519), pp. 1111-1143, 1994.
[26] J. G. Galway, "The Lifted Index as a Predictor of Latent Instability," *Bull. Amer. Meteor. Soc.*, vol. 37, pp. 528–529, 1956.
[27] R. C. Miller, "Notes on analysis and severe-storm forecasting procedures of the Air Force Global Weather Central," AWS Technical Report 200 (rev.), Air Weather Service (MAC), U.S. Air Force, pp. 190, 1972.
[28] Kirshbaum, D. J., et al., *Moist Orographic Convection: Physical Mechanisms and Links to Surface-Exchange Processes*, Atmosphere, 9(3), 80, 2018.
[29] F. Robinson., "Investigating the effects of orography and ambient wind on convective initiation over complex terrain," *Journal of the Atmospheric Sciences*, 2025.
[30] B. Markova, and R. Mitzeva, "Instability Indices as an Indicator of Thunderstorms in Eastern Bulgaria - Preliminary Results", *Bulgarian Geophysical Journal*, 38(13), pp. 12–20, 2012.
[31] Engerer, N. A., Stensrud, D. J., & Coniglio, M. C. "Surface Characteristics of Observed Cold Pools," *Monthly Weather Review*, 136(12), 4839-4849, 2008.